Contents lists available at AccScience Publishing
Nonlinear Science and Control Engineering (NSCE)
Vol. 2, No. 1 (2026)
https://accscience.com/journal/nsce

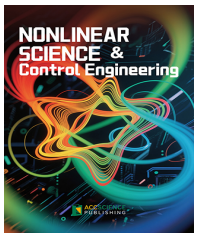

Theoretical analysis and microcontroller-based design of a cyclic network of three mutually coupled Duffing oscillators

Mahirakhon Rakhmatullaeva[1], Khabibullo Nosirov[2], Kengne Jacques[3]*, and Chedjou Jean Chamberlain[4]

[1]*Department of Information Technology, Faculty of Computer Engineering, Tashkent University of Information Technologies, Tashkent, Uzbekistan*
[2]*Department of Television and Radio Broadcasting Systems, Faculty of Information Technologies, Tashkent University of Information Technologies, Tashkent, Uzbekistan*
[3]*Research Unit in Automation and Applied Computer Science (UR-AIA), Department of Electrical Engineering, University Institute of Technology, Fotso Victor, Bandjoun, Koung-Khi, Cameroon*
[4]*Transportation Informatics Group (TIG), Department of Information Technology, Faculty of Technical Sciences, University of Klagenfurt, Austria*

Article History:
Received: November 2, 2025
Revised: December 27, 2025
Accepted: January 5, 2026
Published online: February 4, 2026

ABSTRACT

Recently, coupled oscillator systems have garnered significant interest due to their rich dynamics and applications in various fields. This article examines the collective dynamics of a ring network comprising three mutually interacting autonomous Duffing oscillators. Analytical and numerical methods are employed to elucidate the network's overall behavior as a function of its parameters. We show that the route leading to multi-scroll chaos begins with a series of Hopf bifurcations (associated with 8 of the 27 equilibrium points), followed by a sequence of period-doubling bifurcations, boundary crises, and merging crises, ultimately giving rise to a multi-scroll attractor as one of the system parameters (e.g., a coupling strength) is varied. This route is characterized by several regions of multi-stability, where multiple attractors of different topologies coexist in varying numbers, depending on the exact value of the control parameter. This mechanism is elucidated using key analytical tools, such as bifurcation diagrams, phase portraits, and basins of attraction corresponding to competing attractors. Reducing the number of interactions within the network led to profound modifications in the locations of the equilibrium points, the mechanisms underlying the onset of chaos, and the topology of the resulting multi-scroll attractor. An experimental validation is carried out by considering a physical implementation of the model using the Arduino microcontroller. This study provides valuable insights that serve as an introduction to understanding the dynamics of significantly more complex networks of Duffing oscillators.

Keywords: Heterogeneous multi-stability; Microcontroller-based realization; Ring network of Duffing oscillators; Route to multi-scroll chaos

***Corresponding author**:
Kengne Jacques (kengnemozart@yahoo.fr).

Citation:
Rakhmatullaeva M, Nosirov K, Jacques K, Chamberlain CJ. Theoretical analysis and microcontroller-based design of a cyclic network of three mutually coupled Duffing oscillators. *Nonlinear Sci Cont Eng.* 2026;2(1):025440016. doi: 10.36922/NSCE025440016

1. Introduction

The study of coupled systems is an ongoing research avenue in nonlinear science, with the goal of understanding and predicting the behavior of complex systems through the use of mathematical models. Systems in real life (for instance, networks) can exhibit a large, and sometimes infinite, number of degrees of freedom, which render the modeling process extremely complex.[1,2] Such systems are endowed with rich and striking features, such as chaos, hyperchaos, multi-stability, synchronization, chimera states, oscillation death, intermittency, and hysteresis.[2,3] Studying the dynamics of much smaller networks is sufficient to obtain good agreement between experimentally collected data and the model.[4] The results obtained can be applied to various scientific domains, including engineering, chemistry, physics, medicine, ecology, biology, and economics. In a network, the nodes can interact bi-directionally or unidirectionally, linearly or nonlinearly, and can be organized in different topologies, such as star coupling, ring coupling, chain coupling, or combinations of these basic coupling schemes.[5,6] The Duffing equation, first introduced by Duffing,[7] has been applied in both theoretical and experimental studies by many researchers owing to its ability to describe various nonlinear phenomena.

The dynamics of coupled Duffing oscillators (DO) driven by an external periodic drive have been extensively investigated, whereas less is known about coupled excitation-free DO, despite their theoretical and practical importance. Notably, there has been some interesting work on the dynamics of coupled DO. Tchakui and Woafo[8] discussed the chaos mechanism of three coupled single-well DOs, distinguishing between the ring and chain topologies by considering both configurations. Kingston et al.[9] described a general scenario leading to the emergence of hyperchaos with a sudden large expansion of the attractor size of continuous dynamic systems (e.g., three coupled DO) at a critical parameter value, when the temporal dynamics experienced intermittent large-amplitude spiking or bursting events. Sabarathinam and Thamilmaran[10] reported transient chaos in a ring and a globally coupled system of nearly conservative Hamiltonian DO. Jaimes-Reátegui et al.[11] studied the occurrence of synchronization in the network motif of three bi-stable DO coupled in all possible configurations. The most complex dynamics occurred in the unidirectional chain, where a transition to quasi-periodicity was observed. Musielak et al.[12] reported new findings on the routes to chaos in increasingly complex DO systems, which are formed by coupling several oscillators. Clerc et al.[13] reported the occurrence of chimera states in an array of identical DO coupled to their nearest neighbors. Jothimurugan et al.[14] investigated the resonance behavior in a system composed of n-coupled DOs where only the first oscillator was driven by a periodic force, assuming a nearest-neighbor coupling. Jaros et al.[15] examined the dynamics of a ring of three one-way coupled single-well DO with a polynomial coupling function of degree 3, focusing on the influence of coupling factors on different bifurcation mechanisms. Borkowski et al.[16] reported the experimental observation of a three-frequency quasi-periodic solution in a ring of unidirectionally coupled single-well DOs. Barba-Franco et al.[17] studied the dynamics of a ring of three coupled double-well DO for three types of damping coefficients. Balamurali et al.[18] considered the dynamics of two mutually coupled DOs and reported the occurrence of multi-scroll chaos. Notably, instability resulting from coupling represents one of the most important features of systems designed using discrete interacting oscillators.

Motivated by the above works, this study examines the collective behavior of a small network composed of three mutually interacting DOs in a ring topology (RCDO) with the following key objectives:

(i) To investigate the mechanism of multi-scroll chaos generation in the coupled system as a function of both the dissipation and the coupling factors.
(ii) To evaluate the effects generated by the successive removal of the coupling coefficients on the bifurcation modes, the different forms of multi-stability, as well as the topology of the chaotic multi-scroll attractor in the network.
(iii) To design a microcontroller-based hardware model to demonstrate the practical feasibility of the dynamic properties observed in theoretical studies.

The remainder of the article is divided into four sections. Section 2 presents the mathematical properties of a ring network of three mutually coupled DOs. The basic network properties are examined analytically in terms of fixed points, Hopf bifurcations, symmetry, energy transfer, and dissipation. Section 3 presents the results of the numerical investigation connected to the mechanism of the multi-scroll chaos, focusing on the impact of coupling coefficients. Hardware digital implementation of the network is considered in Section 4 to confirm the salient features exhibited by the network model. Section 5 summarizes the results and underlines challenges to be addressed in future studies.

2. The network model and properties

2.1. State equations

We considered three mutually coupled twin-well DO (Figure 1) whose mathematical model can be formulated as a collection of three coupled second-order ordinary differential equations (Equations (1)–(3)):

$$\ddot{x} = x + \alpha y - \beta_3 z - (x + \alpha y - \beta_3 z)^3 - \delta \dot{x} \tag{1}$$

$$\ddot{y} = y - \beta_1 x + \alpha z - (y - \beta_1 x + \alpha z)^3 - \delta \dot{y} \tag{2}$$

$$\ddot{z} = z + \alpha x - \beta_2 y - (z + \alpha x - \beta_2 y)^3 - \delta \dot{z} \tag{3}$$

Here, the over dots stand for the time derivative α and $\beta_n\,(n = 1, 2, 3)$ are the coupling coefficients, while δ represents the (linear) dissipation. In the network of DO governed by Equations (1)–(3), it is evident that the amplitude of one node oscillator evolves according to the amplitude of its nearest neighboring cells. Notably, the interaction adopted is of a nonlinear type.[18–21] If we adopt $u = \dot{x}$, $v = \dot{y}$, and $w = \dot{z}$, it is possible to rewrite the three RCDO Equations (1)–(3) using a set of six coupled first-order ordinary differential equations of order:

$$\dot{x} = u \tag{4}$$

$$\dot{u} = x + \alpha y - \beta_2 z - (x + \alpha y - \beta_2 z)^3 - \delta u \tag{5}$$

$$\dot{y} = v \tag{6}$$

$$\dot{v} = y - \beta_1 x + \alpha z - (y - \beta_1 x + \alpha z)^3 - \delta v \tag{7}$$

$$\dot{z} = w \tag{8}$$

$$\dot{w} = z + \alpha x - \beta_2 y - (z + \alpha x - \beta_2 y)^3 - \delta w \tag{9}$$

Each of the three DOs is independent and uncorrelated to the two others for zero coupling parameters (i.e., $\alpha = \beta_k = 0$ $[k = 1, 2, 3]$). Accordingly, each individual DO did not experience any oscillations. Notably, the coupling term received by each DO acts as an effective forcing term in the absence of an external periodic drive, which accounts for the rich dynamics observed in the entire network.

Notably, Equations (4)–(9) present only cubic nonlinearities, indicating that they are odd symmetric. Likewise, the corresponding Lie derivative is always negative (Equation (10)):

$$\frac{1}{V}\frac{dV}{dt} = \frac{\partial \dot{x}}{\partial x} + \frac{\partial \dot{y}}{\partial y} + \frac{\partial \dot{z}}{\partial z} + \frac{\partial \dot{p}}{\partial p} + \frac{\partial \dot{u}}{\partial u} + \frac{\partial \dot{v}}{\partial v} + \frac{\partial \dot{w}}{\partial w} + \frac{\partial \dot{q}}{\partial q} = -4\delta < 0 \tag{10}$$

Hence, the ring network Equations (4)–(9) were considered dissipative and can be used to develop attractors accordingly.[22,23] Alternatively, the coupled Duffing Equations (4)–(9) can be analyzed using an energy balance. On this line, Equation (5) was multiplied by u, Equation (7) by v , and Equation (9) by w; then summing the three results yielded the expressions of the network energy and the first time derivative dH/dt :

$$H = \frac{1}{4}\left(x^4 - 2x^2 + 2u^2 + y^4 - 2y^2 + 2v^2 + z^4 - 2z^2 + 2w^2\right) \tag{11}$$

$$\frac{dH}{dt} = dH_1 + dH_2 + dH_3 \tag{12}$$

$$dH_1 = -\delta u^2 + u\left(\alpha y - \beta_3 z\right)\left(1 + 3x^2 + 3x\left(\alpha y - \beta_3 z\right) + \left(\alpha y - \beta_3 z\right)^2\right) \tag{13}$$

$$dH_2 = -\delta v^2 + v\left(\alpha z - \beta_1 x\right)\left(1 + 3y^2 + 3y\left(\alpha z - \beta_1 x\right) + \left(\alpha z - \beta_1 x\right)^2\right) \tag{14}$$

$$dH_3 = -\delta w^2 + w\left(\alpha x - \beta_2 y\right)\left(1 + 3z^2 + 3z\left(\alpha x - \beta_2 y\right) + \left(\alpha x - \beta_2 y\right)^2\right) \tag{15}$$

From the above equations, we deduce that the time evolution of energy in the coupled DO system has a strong dependence on the work defined by the values of the coupling factors and the phasing as well.

2.2. Analysis of the fixed points

The static solutions of the small RCDO systems in Equations (4)–(9) were reached by setting all time derivatives (i.e.., $\dot{u} = \dot{v} = \dot{w} = 0$, $\dot{x} = \dot{y} = \dot{z} = 0$) and solving the resulting algebraic equations.[22,23] Hence, any fixed point meets $w = v = u = 0$ and the elongation variables x, y, and z fulfil a three-variable system:

$$x + \alpha y - \beta_3 z - (x + \alpha y - \beta_3 z)^3 = 0 \tag{16}$$

$$y - \beta_1 x + \alpha z - (y - \beta_1 x + \alpha z)^3 = 0 \tag{17}$$

$$z + \alpha x - \beta_2 y - (z + \alpha x - \beta_2 y)^3 = 0 \tag{18}$$

Table 1 presents the analytical expressions of the 27 equilibrium points of the RCDO system in Equations (4)–(9). Notably, we discarded the critical situation $1 - \alpha_1\beta_1 - \alpha_2\beta_2 = 0$ for which the coupled system degenerates and admits an infinite number of equilibrium points. In the neighborhood of the point $M(x, u, y, v, z, w)^T$ in the state space,[22,23] the linearization of Equations (4)–(9) generates the Jacobian matrix:

$$M_J = \begin{bmatrix} 0 & 1 & 0 & 0 & 0 & 0 \\ \vartheta_1 & -\delta & \alpha\vartheta_1 & 0 & -\beta_1\vartheta_1 & 0 \\ 0 & 0 & 0 & 1 & 0 & 0 \\ -\beta_1\vartheta_2 & 0 & \vartheta_2 & -\delta & \alpha\vartheta_2 & 0 \\ 0 & 0 & 0 & 0 & 0 & 1 \\ \alpha\vartheta_3 & 0 & -\beta_2\vartheta_3 & 0 & \vartheta_3 & -\delta \end{bmatrix} \tag{19}$$

$$\vartheta_1 = 1 - 3(x + \alpha y - \beta_3 z)^2, \vartheta_2 = 1 - 3(y + \alpha z - \beta_1 x)^2, \vartheta_3 = 1 - 3(z + \alpha x - \beta_2 y)^2 \tag{20}$$

Based on the above expression of the Jacobian matrix, we discuss the linear stability of any equilibrium $E_n(x_n, 0, y_n, 0, z_n, 0)^T$ according to the Routh–Hurwitz criterion. At any position E_n, the characteristic polynomial $Q(\lambda) = \det(M_J - \lambda I_d)$ (I_d the 6×6 identity matrix) has the form:

$$Q(\lambda) = \lambda^6 + k_5\lambda^5 + k_4\lambda^4 + k_3\lambda^3 + k_2\lambda^2 + k_1\lambda + k_0 \tag{21}$$

$$k_5 = 3\delta \tag{22}$$

$$k_4 = 3\delta^2 - \sum_{k=1}^{3}\vartheta_k \tag{23}$$

$$k_3 = \delta^3 - 2\delta\sum_{k=1}^{3}\vartheta_k \tag{24}$$

$$k_2 = \sum_{j\neq k}\vartheta_k\vartheta_j - \delta^2\sum_{k=1}^{3}\vartheta_k + \alpha\left(\beta_1\vartheta_1\vartheta_2 + \beta_2\vartheta_2\vartheta_3 + \beta_3\vartheta_1\vartheta_3\right) \tag{25}$$

$$k_1 = \delta\sum_{j\neq k}\vartheta_k\vartheta_j + \alpha\delta\left(\beta_1\vartheta_1\vartheta_2 + \beta_2\vartheta_2\vartheta_3 + \beta_3\vartheta_1\vartheta_3\right) \tag{26}$$

$$k_0 = \vartheta_1\vartheta_2\vartheta_3\left(\beta_1\beta_2\beta_3 - \alpha^3 - \alpha\beta_1 - \alpha\beta_2 - \alpha\beta_3 - 1\right) \tag{27}$$

In Table 1, we compiled the analytical expressions of the equilibrium points, the characteristic polynomials associated with each of these points according to the network's parameters, as well as the type of stability. According to the information presented in Table 1, we can distinguish two categories of equilibrium points: those that are always unstable (i.e., $E_n[n = 0, 9 \ldots 26]$) and those whose stability changes with the variation of the network parameters, namely E_n $(n = 1 \ldots 8)$. This latter category shares the same characteristic polynomial (Table 1) and therefore undergoes a Hopf bifurcation at the same critical parameter value (e.g., the dissipation δ, a coupling

coefficient $\beta_n[n = 1, 2, 3]$). The Hopf bifurcation occurs simultaneously for eight equilibrium points, giving rise to eight parallel bifurcation branches.

3. Multi-scroll chaos mechanism

3.1. Numerical computation scheme

In this section, we proceed to the numerical study of the collective dynamics of the network of three DO described by the system in Equations (4)–(9). We used the Runge–Kutta numerical integration method[22,23] of order four, considering a fixed time step $\Delta t = 2 \times 10^{-3}$. For each fixed value of the bifurcation parameter, the system described in Equations (4)–(9) was numerically integrated, and the solutions were recorded after a sufficiently long time to discard the transient effects. The mutual coupling coefficients were set to zero one at a time to assess their influence on the collective dynamics of the network. Particular attention was also paid to the impact of the dissipation parameter. Three special cases were distinguished. To enhance our understanding of the collective dynamics of the coupled system as a specific parameter changes, we utilized a combination of three graphical methods: the Lyapunov exponent spectrum, bifurcation diagrams, and phase portrait plots. Given that the system exhibited numerous attractors at specific parameter values, the initial conditions were derived by applying the equations in Table 1 (i.e., $E_n[n = 1, 3, 5, 7]$), which defined certain equilibrium points within our integration algorithm, while incorporating a small initial velocity (e.g., $u(0) = 0.1$; $v(0) = w(0) = 0$). When multiple attractors exist for the same parameter range, each attractor crosses a distinct region of the state space unique to it. This criterion facilitates the identification of the various basins of attraction. Recall that the term basin of attraction refers to the set of initial conditions in a dynamical system that lead to a particular attractor as time progresses.

3.2. Dynamics in the case $\beta_2 = \beta_3 = 0$

Figure 2 displays four of the eight coexisting bifurcation branches (Figure 2a) for the process of multi-spiral creation in the ring network of DO when the dissipation δ was swept downward from the four initial values. Three of these branches vanished as the parameter decreased due to basin collapse at specific critical values unique to each branch. We plotted the variation of the maximum Lyapunov exponent, denoted as Lya (Figure 2b), connected to each of the coexisting branches of bifurcation using the same set of colors in Figure 2a. Other parameters employed for the computations were selected as $\alpha = \beta_1 = 0.6$ and $\beta_2 = \beta_3 = 0$. For this parameter setting, we reported (Figure 3) diverse types of competing behaviors occurring with varying dissipation consisting, for example, of eight period-1 cycles for (Figure 3a); four chaotic attractors and four period-1 cycles for $\delta = 0.835$(Figure 3c); a pair of two-scroll and a pair of one-scroll chaotic attractors for $\delta = 0.68$ (Figure 3e); two pairs of two-scroll chaotic attractors for (Figure 3g); and a single eight-scroll chaotic attractor for $\delta = 0.55$ (Figure 3i). Figure 3b, d, f, h, and j shows related basins of attraction using the same set of colors. To provide further information about the complexity of the coupled system, we produced (Figure 4) several two-dimensional views of the eight-scroll chaotic attractor (Figure 4a–d) depicted in Figure 3i and the projection of the same attractor in the (x, y, z) space (Figure 4e). These plots serve to better highlight the non-trivial topology of the eight-scroll attractors. We also examined how the system dynamics are affected by dissipation. Accordingly, four of the eight coexisting bifurcation trees (Figure 5a) associated with multi-spiral formation in the ring network of Duffing oscillators were obtained when the dissipation parameter δ was swept downward from the four sample initial values. Three of these branches vanished as the parameter decreased due to basin collapse at branch-specific critical values. We plotted the variation of the Lyα exponent (Figure 5b) connected to each of the coexisting branches of bifurcation using the same set of colors in Figure 5a. For the latter computations, we fixed $\alpha = 0.6$, $\beta_1 = 0.6$, and $\beta_2 = 0.60$.

3.3. Dynamics in the case $\beta_3 = 0$

The case $\beta_3 = 0$ corresponds to the absence of mutual interaction between the node oscillators labeled X and Z (Figure 1), whereas coupling is maintained between X and Y and between Y and Z. Setting the coupling factors $\alpha = \beta_1 = \beta_2 = 0.60$, and $\beta_3 = 0$ resulted in diverse types of competing behaviors (Figure 6) with varying dissipation, such as eight period-1 cycles for $\delta = 1.15$ (Figure 6a); four chaotic attractors, two period-1 cycles, and two period-4 cycles for $\delta = 0.948$ (Figure 6c); two mutually symmetric four-scroll chaotic attractors for $\delta = 0.75$ (Figure 6e); and an eight-scroll chaotic attractor for $\delta = 0.65$ (Figure 6g). Figure 6b, d, f, and h shows related basins of attraction using the same set of colors. Notably, there was a change in the positions (in phase space) of the equilibrium points and related limit cycle after the Hopf bifurcation, as well as the topology of the final chaotic attractor, compared to the case discussed in the previous section.

3.4. Dynamics in the case $\beta_1 = \beta_2 = \beta_3 \neq 0$

The case $\beta_1 = \beta_2 = \beta_3 \neq 0$ corresponds to the situation where the three-node oscillators interact mutually in the ring network. The collective dynamics that evolve from the network are illustrated in Figure 7. More explicitly, Figure 7 presents four of the eight coexisting trees of bifurcation (Figure 7a) for the process of multi-spiral creation in the ring network of DO when the dissipation δ was swept downward from the four initial values. Three of these branches vanished as the parameter decreased due to basin collapse at branch-specific critical values. We plotted the variation of the Lyα (Figure 7b) exponent connected to each of the coexisting branches of bifurcation using the same set of colors in Figure 7a. For these computations, we fixed $\alpha = 0.6$ and $\beta_1 = \beta_2 = \beta_3 = 0.6$. Diverse types of competing behaviors occurred in this mode of operation with varying dissipation, such as eight period-1 cycles for $\delta = 1.25$ (Figure 8a); six chaotic attractors and two period-1 cycles for $\delta = 1.025$ (Figure 8c); two mutually symmetric mono-scroll chaotic attractors with a six-scroll chaotic attractor for $\delta = 0.81$ (Figure 8e); and an eight-scroll chaotic attractor for $\delta = 0.75$ (Figure 8g). Figure 8b, d, f, and h shows related basins of attraction using the same set of colors. Zones of unbounded dynamics are marked yellow. As mentioned previously, the distribution of the equilibrium points, the location of the limit cycle, and the topology of the multi-scroll chaotic (here, a six-scroll attractor) are different from the two cases discussed previously.

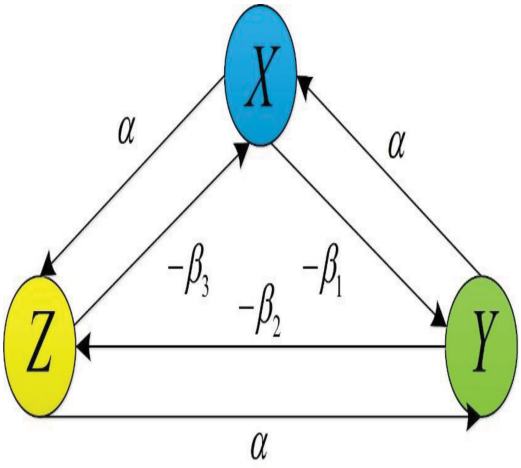

Figure 1. The small network of three mutually interacting Duffing oscillators denoted by X, Y, and Z. and β_k $(k = 1, 2, 3)$ represents the coupling coefficients. A unidirectional ring was obtained in case $\beta_k = 0$ $(k = 1, 2, 3)$.

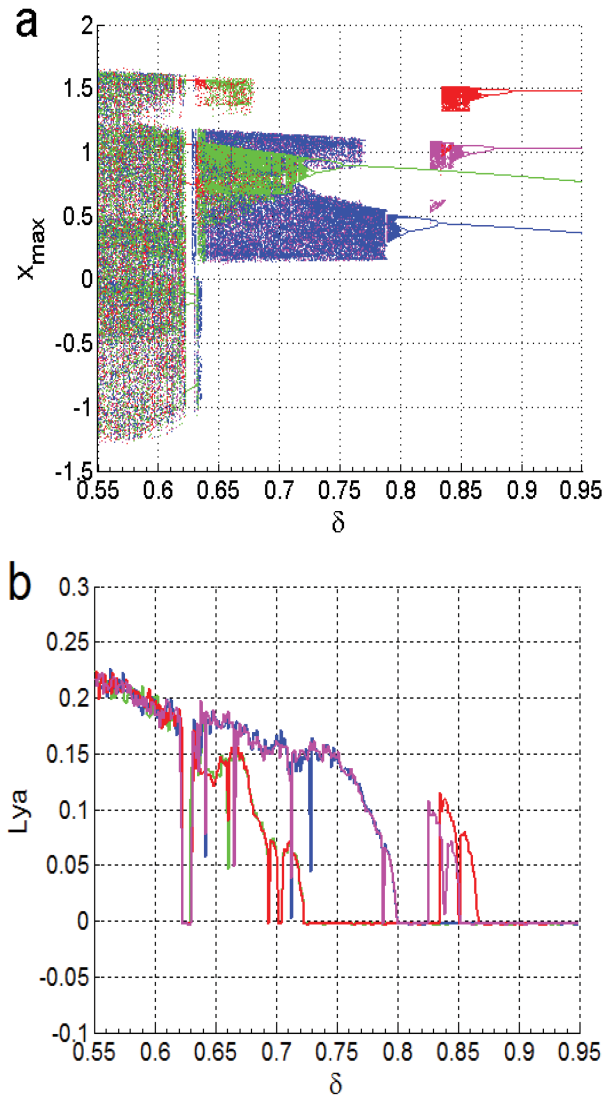

Figure 2. Four of the eight coexisting trees of bifurcation. (a) The process of multi-spiral creation in the ring network of DO when the dissipation δ is swept downward from four initial values near E_1 (red), E_3 (magenta), E_5 (green), E_7 (blue). (b) The variation of the maximum Lyapunov exponent (Lya) connected to each of the coexisting branches of bifurcation using the same set of colors in (a). Other parameters employed for the computations are fixed: $\alpha = \beta_1 = 0.6$ and $\beta_2 = \beta_3 = 0$.

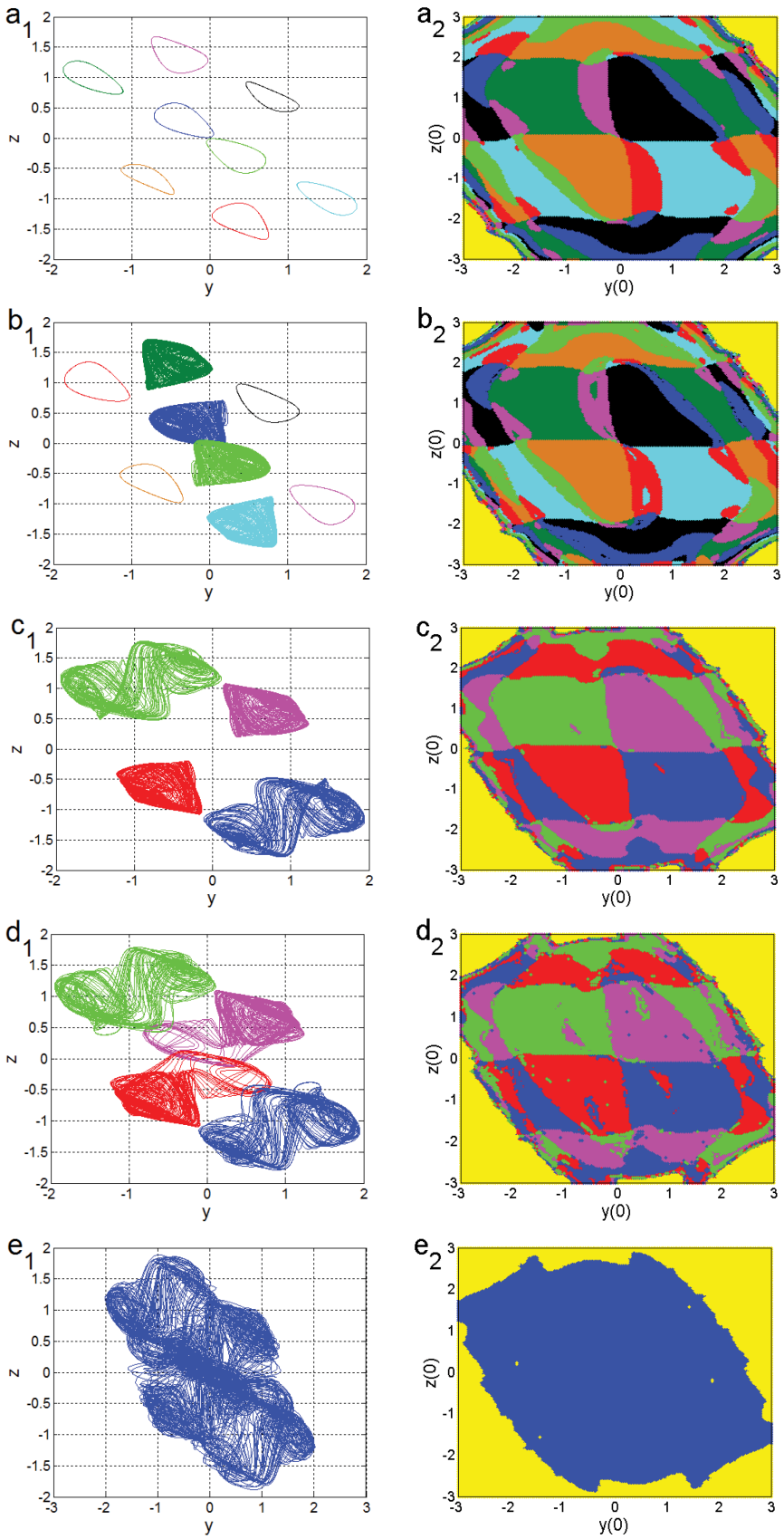

Figure 3. The resulting diverse types of competing behaviors with varying dissipation after setting the coupling factors to $\alpha = \beta_1 = 0.60$ and$\beta_2 = \beta_3 = 0$. (a) Eight period-1 cycles for $\delta = 0.95$. (c) Four chaotic attractors and four period-1 cycles for $\delta = 0.835$. (e) A pair of two-scroll and a pair of one-scroll chaotic attractors for $\delta = 0.68$. (g) Two pairs of two-scroll chaotic attractor for $\delta = 0.65$. (i) A single eight-scroll chaotic attractor for $\delta = 0.55$. (b, d, e, f, h, j) Related basins of attraction using the same set of colors.

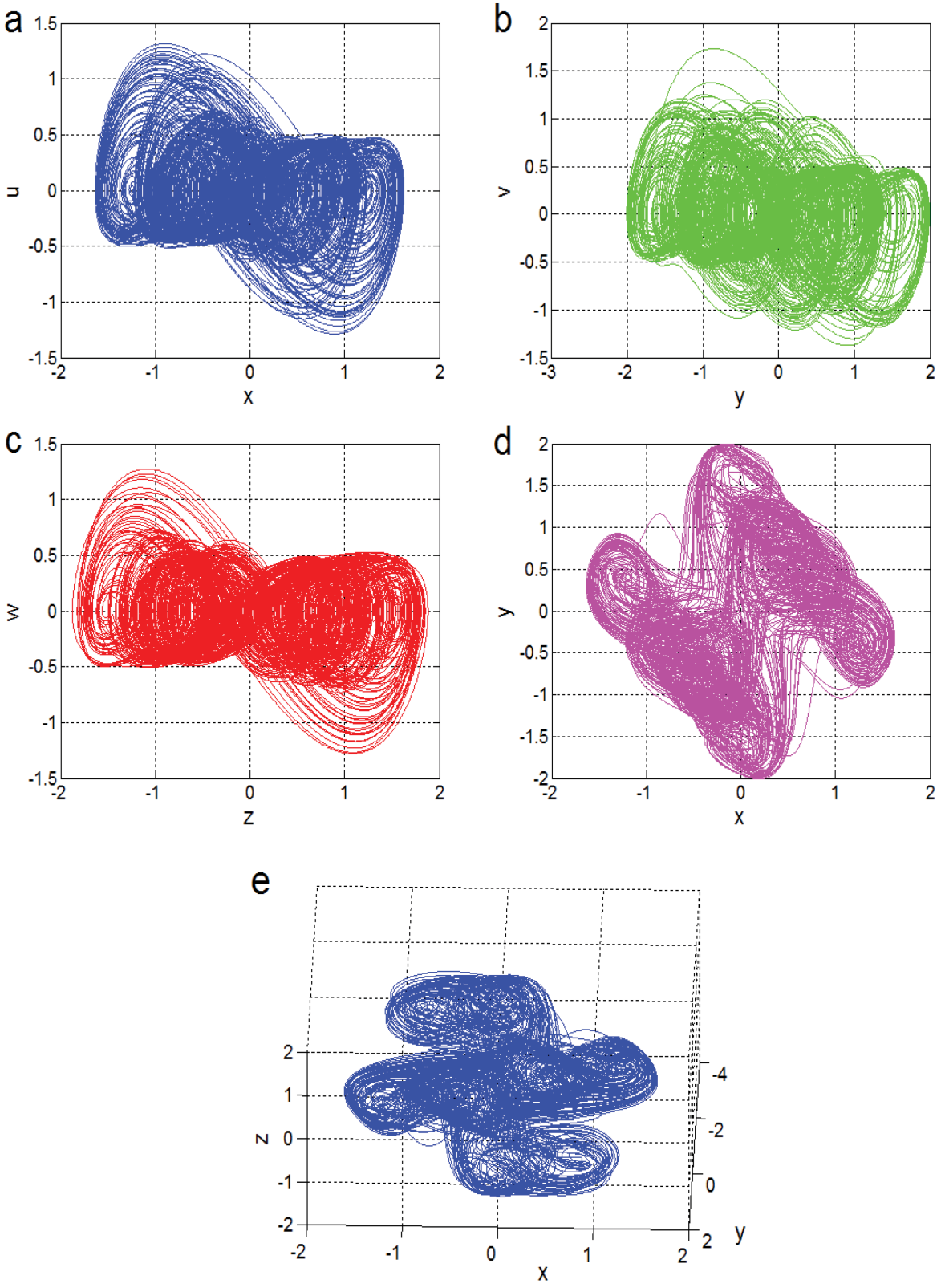

Figure 4. Two-dimensional views of the eight-scroll chaotic attractor. (a, b, c, d) Views of the attractor depicted in Figure 3i and (e) the projection of the same attractor in the (x, y, z) space. These plots provide additional information connected to the topology of the underlying eight-scroll attractor.

4. Microcontroller-based implementation

It is recognized that various techniques exist for performing analog simulations of the coupled system model analyzed in this study, including analog computation, field-programmable gate array cards, and microcontroller boards. The decision to use Arduino boards in this research is driven by their straightforward implementation and versatility. The digital electronic design of the three DO system in Equations (4)–(9) using an ATMEGA2560-type microcontroller (Microchip Technology Inc., USA) was

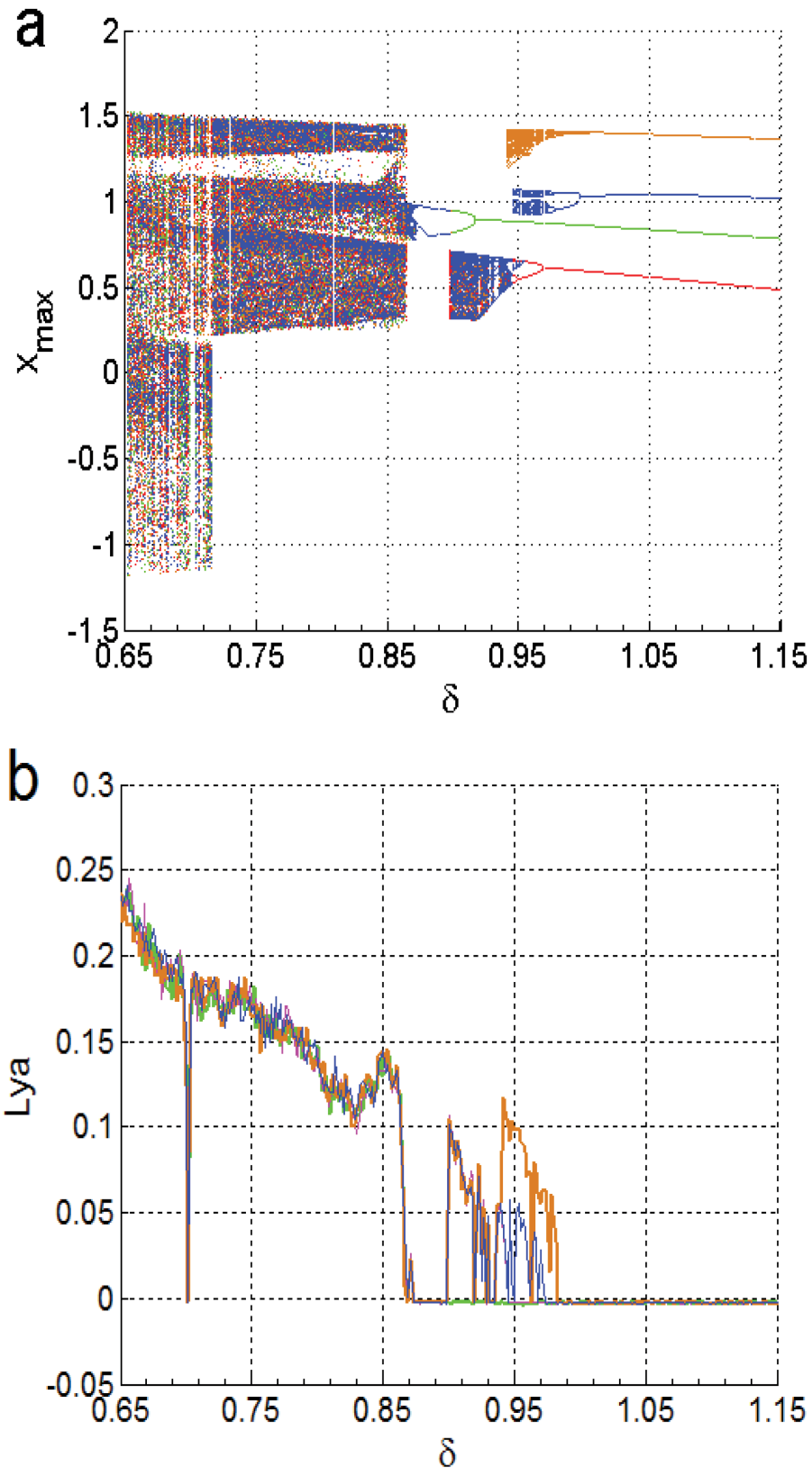

Figure 5. Four of the eight coexisting trees of bifurcation. (a) The process of multi-spiral creation in the ring network of DO when the dissipation is swept downward from four initial values near E_1 (red), E_3 (blue), E_5 (magenta), E_7 (green). (b) The variation of the maximum Lyapunov exponent (Lya) connected to each of the coexisting branches of bifurcation using the same set of colors in (a). Other parameters employed for the computations are fixed: $\alpha = 0.6$, $\beta_1 = 0.6$, and $\beta_2 = 0.60$.

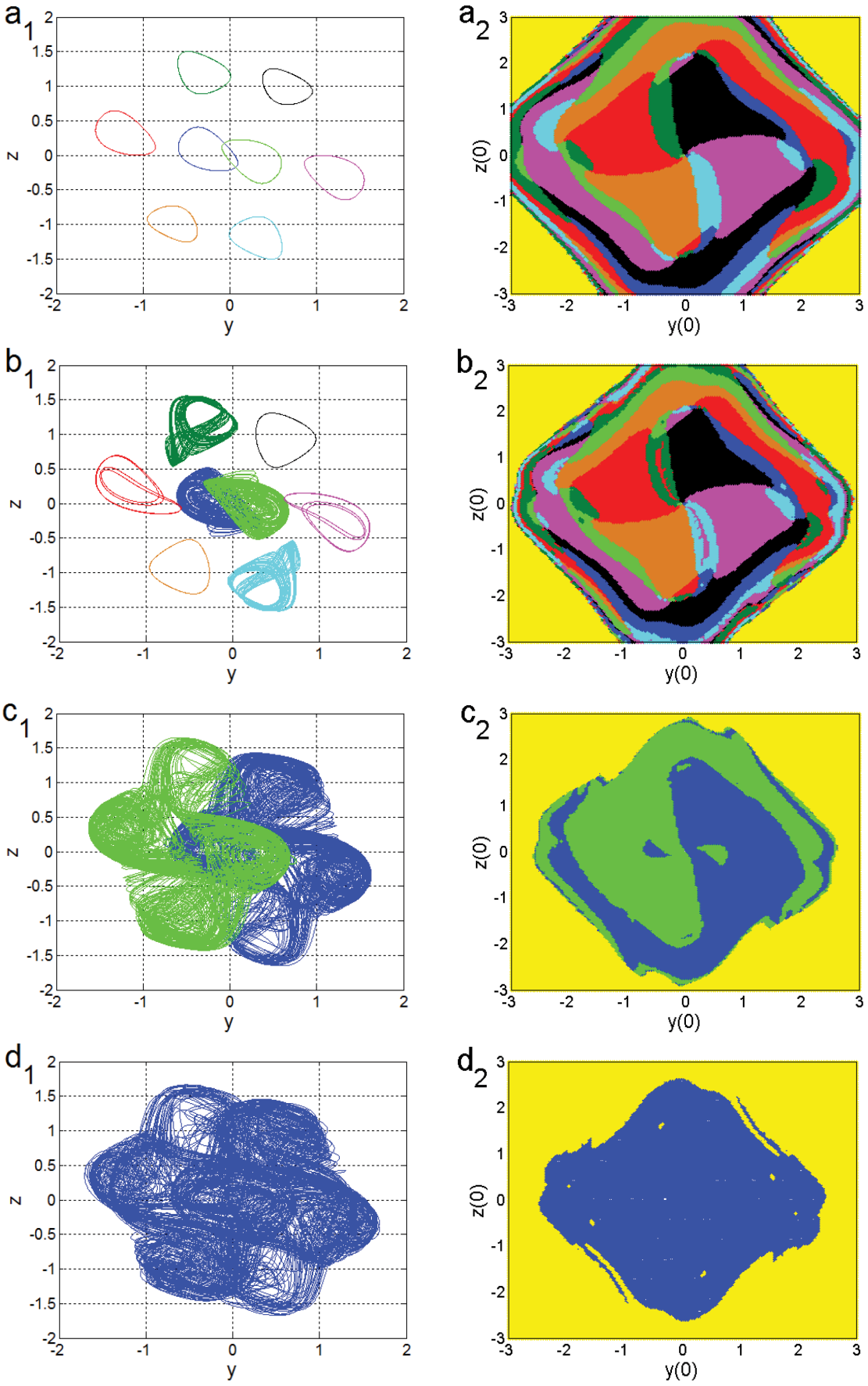

0

Figure 6. The resulting diverse types of competing behaviors with varying dissipation after setting the coupling factors to $\alpha = \beta_1 = \beta_2 = 0.60$, and $\beta_3 = 0$. (a) Eight period-1 cycles for $\delta = 1.15$. (c) Four chaotic attractors, two period-1 cycles, and two period-4 cycles for $\delta = 0.948$. (e) Two mutually symmetric four-scroll chaotic attractors for $\delta = 0.75$. (g) An eight-scroll chaotic attractor for $\delta = 0.65$. (b, d, e, f, h) Related basins of attraction using the same set of colors.

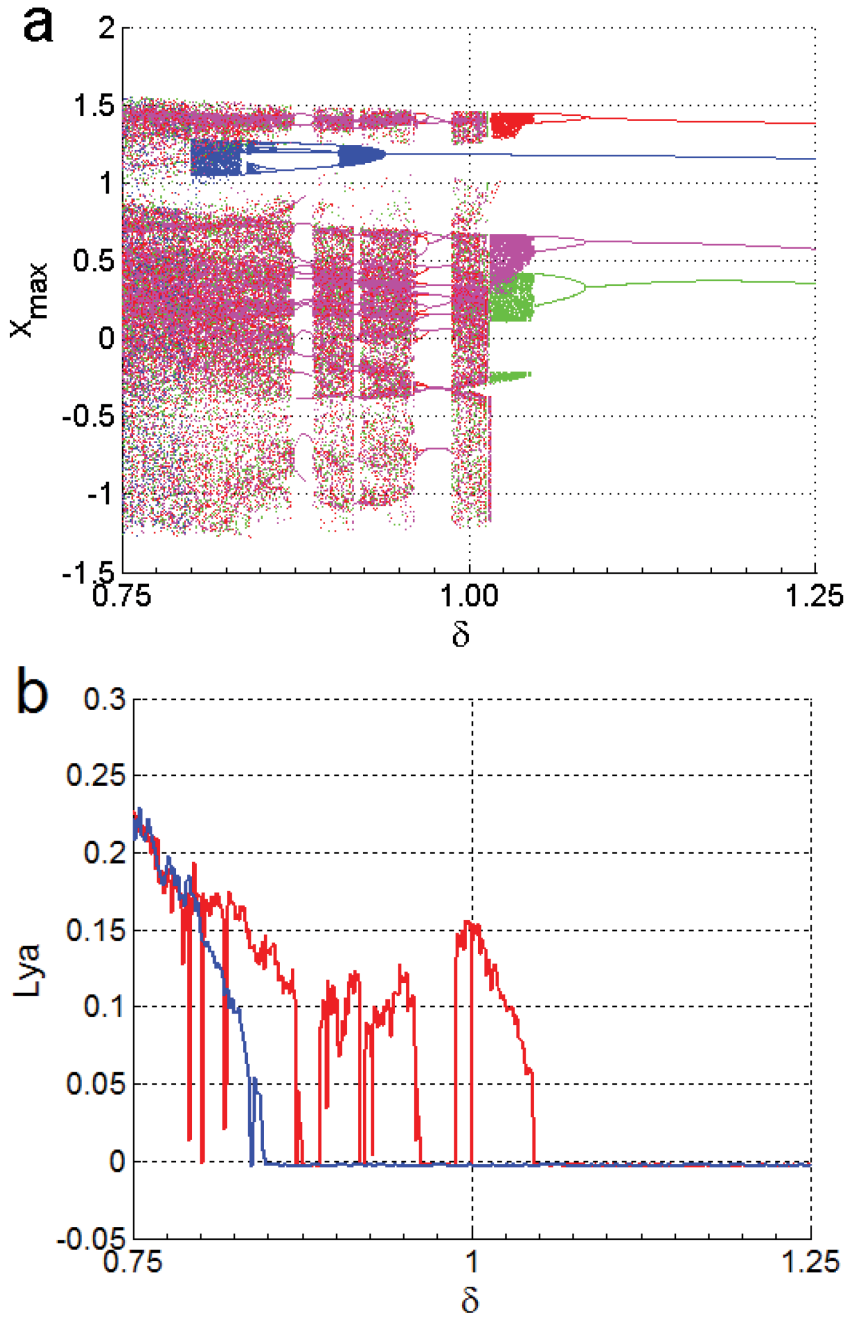

Figure 7. Four of the eight coexisting trees of bifurcation. (a) The process of multi-spiral creation in the ring network of DO when the dissipation δ is swept downward from four initial values nearE_1 (red), E_3 (blue), E_5 (magenta), E_7 (green). (b) The maximum Lyapunov exponent (Lya) connected to each of the coexisting branches of bifurcation using the same set of colors in (a). Other parameters employed for the computations are fixed: $\alpha = 0.6$ and $\beta_1 = \beta_2 = \beta_3 = 0.6$.

achieved, as exemplified by the photograph of the experimental setup and the block diagram included in Figure 9a and b. The microcontroller platform is low-cost, simple, and enables precise control of parameters and initial conditions. The code used to solve the network Equations (4)–(9) according to the fourth-order RK4 method is transferred from the computer to the Arduino Mega 2560 module (Microchip Technology Inc., USA) via a Universal Serial Bus cable. The microcontroller's output pins (serial clock & serial data) were linked to a pair of MCP4725 modules (12-bit digital-to-analog converters) following the serial communication scheme. The converter outputs were visualized simultaneously using a twin-channel digital oscilloscope (DSO2C10, Qingdao Hantek Electronic Co., Ltd., China). Because the digital-to-analog converter module operates with input in the range of 0–5 V, a conversion scale was applied internally in the microcontroller's running code. Figure 10 shows the hardware experimental results (Figure 10a–d) of the coexistence of two one-scroll chaotic attractors with two two-scroll chaotic ones realized by using four distinct values of initial states $(0, 0, \pm 0.5, 0, \pm 0.5, 0)$ and $(0, 0, \pm 0.5, 0, \mp 0.5, 0)$, taking $\alpha = 0.6$, $\beta_1 = 0.6$,$\beta_2 = \beta_3 = 0$, and $\delta = 0.68$. The results from a direct numerical integration of the network Equations (4)–(9) are presented in Figure 10e for comparison purposes. Similarly, we

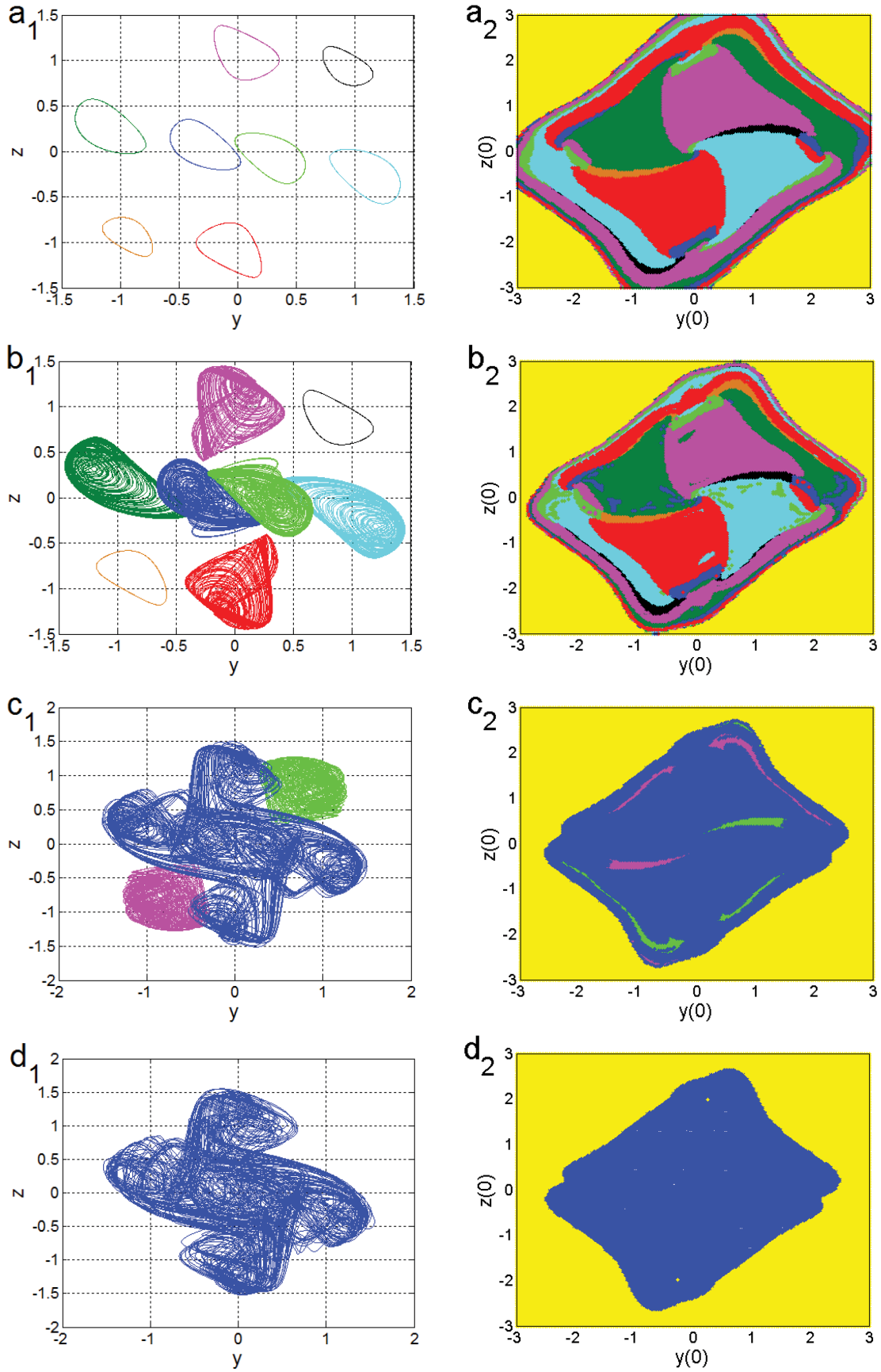

Figure 8. The resulting diverse types of competing behaviors with varying dissipation after setting the coupling factors to $\beta_1 = \beta_2 = \beta_3 = 0.60$ and $\alpha = 0.60$. (a) Eight period-1 cycles for$\delta = 1.25$. (c) Six chaotic attractors and two period-1 cycles for $\delta = 1.025$. (e) Two mutually symmetric mono-scroll chaotic attractors with a six-scroll chaotic attractor for $\delta = 0.81$. (g) An eight-scroll chaotic attractor for $\delta = 0.75$. (b, d, e, f, h) Related basins of attraction using the same set of colors. Zones of unbounded dynamics are marked yellow.

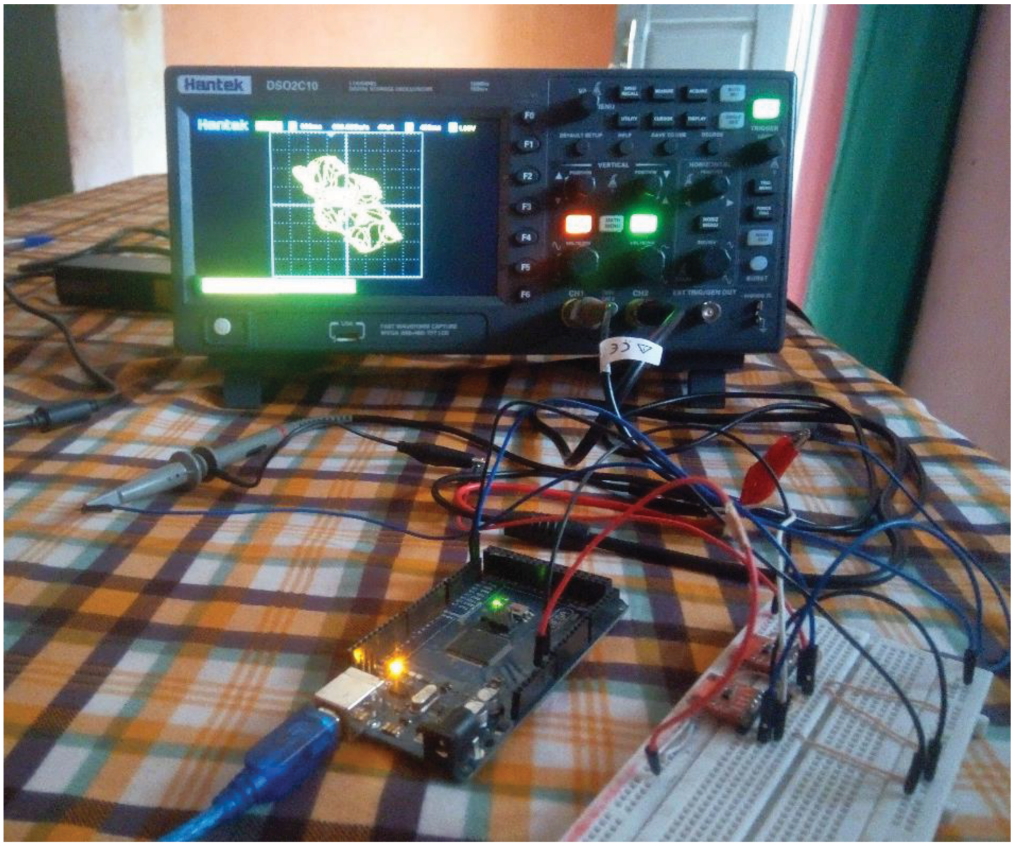

(a)

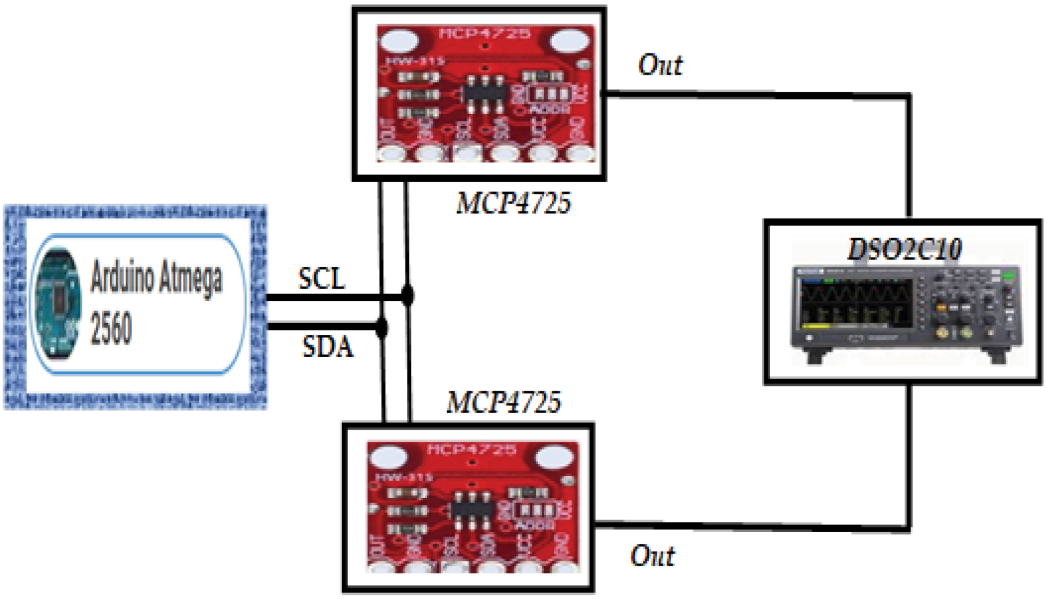

(b)

Figure 9. Experimental setup. (a) The setup consisted of an Arduino Atmega board, a pair of MCP4725-type digital-to-analog converters mounted on a board, and a two-channel digital oscilloscope. (b) A block diagram illustrating the working principle of the whole system. Abbreviations: SCL, serial clock; SDA, serial data.

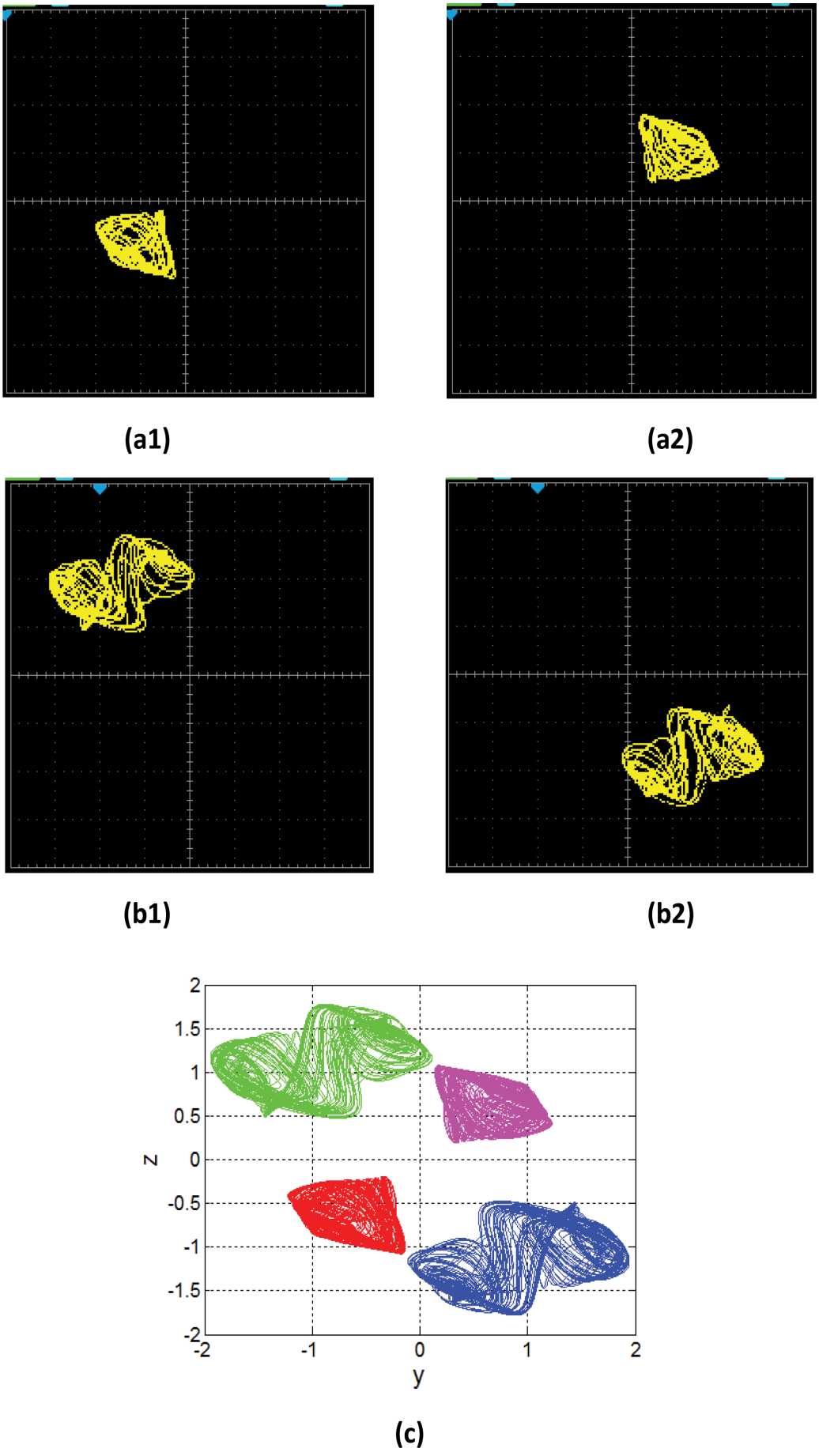

Figure 10. (a–d) Hardware experimental results of the coexistence of two one-scroll chaotic attractors with two 2-scroll chaotic ones, realized using four distinct values of initial states $(0, 0, \pm 0.5, 0, \pm 0.5, 0)$ and $(0, 0, \pm 0.5, 0, \mp 0.5, 0)$ with $\alpha = 0.6$, $\beta_1 = 0.6$, $\beta_2 = \beta_3 = 0$, and $\delta = 0.68$. (e) The results from a direct numerical integration of the network equations.

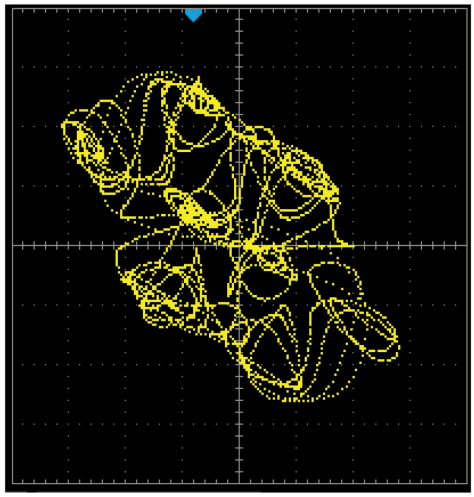

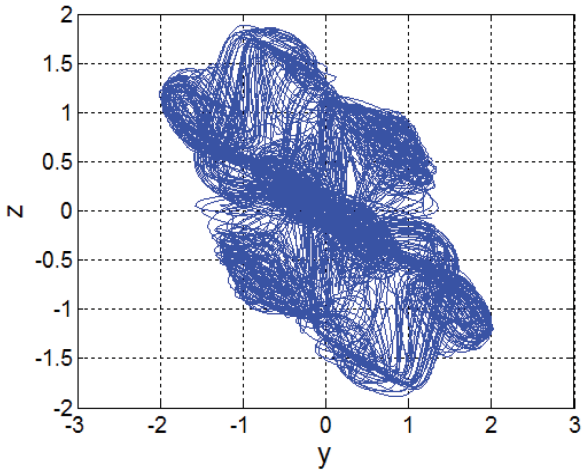

(a1) (a2)

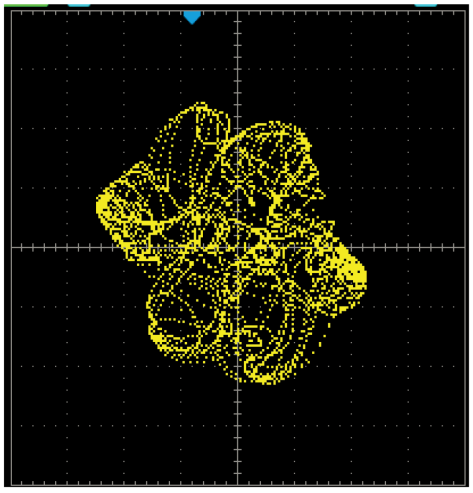

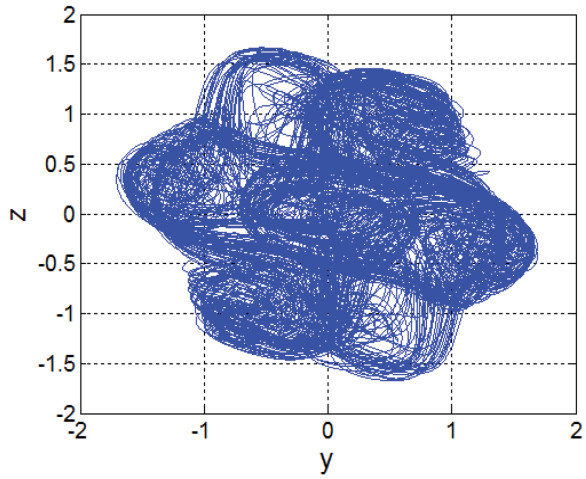

(b1) (b2)

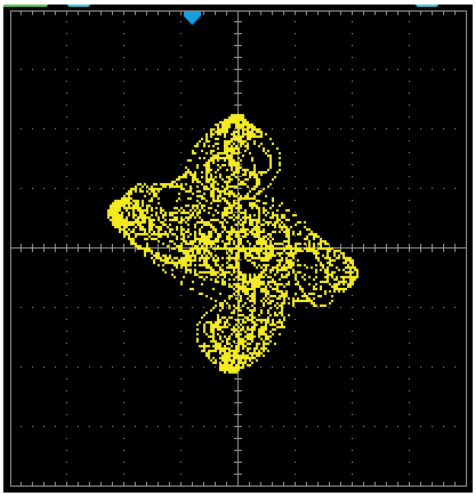

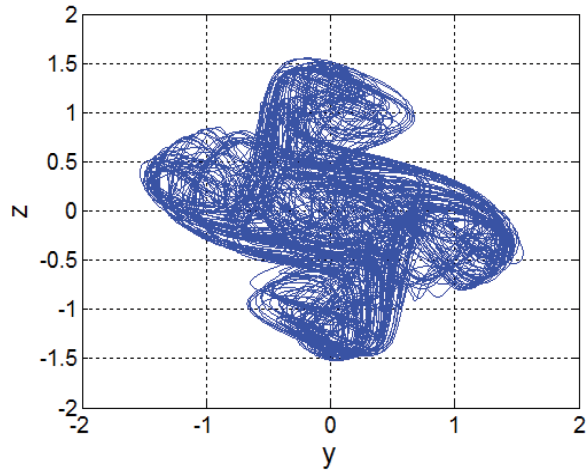

(c1) (c2)

Figure 11. Chaotic attractors captured with a double-channel digital oscilloscope from the Arduino microcontroller-based hardware experiment for three different sets of parameters (a, c, e) and related results (b, d, f) obtained from a direct numerical integration of the network Equations (4)–(9) with the same set of parameters: (a, b) $\alpha = 0.6$, $\beta_1 = 0.6$, and $\beta_2 = \beta_3 = 0$, $\delta = 0.6$; (c, d) $\alpha = 0.6$, $\beta_1 = \beta_2 = 0.6$, $\beta_3 = 0$, and $\delta = 0.6$; (e, f) $\alpha = 0.6$, $\beta_1 = \beta_2 = \beta_3 = 0.6$, and $\delta = 0.6$.

Table 1. The stability properties of the 27 equilibrium positions according to the Routh–Hurwitz criterion

Equilibrium point	**Stability type**
$E_0\,(0,0,0,0,0,0)$	$k_5 = 3\delta$ $k_4 = 3\delta^2 - 3$ $k_3 = \delta^3 - 6\delta$ $k_2 = -3\delta^2 + \alpha\,(\beta_1 + \beta_2 + \beta_3) + 3$ $k_1 = \delta\,(3 + \alpha\beta_1 + \alpha\beta_2 + \alpha\beta_3)$ $k_0 = \beta_1\beta_2\beta_3 - \alpha\beta_2 - \alpha\beta_3 - \alpha^3 - \alpha\beta_1 - 1$ ($k_5k_0 < 0$ unstable)
$E_{1,2}\,(\pm x_1, 0, \pm y_1, 0, \pm z_1, 0)$ $x_1 = \chi\left(1 + \beta_3 - \beta_2\beta_3 + \alpha + \alpha\beta_2 + \alpha^2\right)$ $y_1 = \chi\left(-1 + \beta_1 + \beta_1\beta_3 - \alpha - \alpha\beta_3 + \alpha^2\right)$ $z_1 = 1 - \alpha x_1 + \beta_2 y_1$	$k_5 = 3\delta$ $k_4 = 3\delta^2 + 6$ $k_3 = \delta^3 + 12\delta$ $k_2 = 6\delta^2 + \alpha\,(4\beta_1 + 4\beta_2 + 4\beta_3) + 12$ $k_1 = \delta\,(12 + 4\alpha\beta_1 + 4\alpha\beta_2 + 4\alpha\beta_3)$ $k_0 = 8\alpha\beta_1 + 8\alpha\beta_2 + 8\alpha\beta_3 + 8\alpha^3 - 8\beta_1\beta_2\beta_3 + 8$ ($k_n > 0\,(n = 0,1,2,3,4,5) \Rightarrow$ depends on parameters)
$E_{3,4}\,(\pm x_3, 0, \pm y_3, 0, \pm z_3, 0)$ $x_3 = \chi\left(1 - \beta_3 - \beta_2\beta_3 + \alpha + \alpha\beta_2 - \alpha^2\right)$ $y_3 = \chi\left(-1 + \beta_1 - \beta_1\beta_3 + \alpha - \alpha\beta_3 + \alpha^2\right)$ $z_3 = -1 - \alpha x_3 + \beta_2 y_3$	
$E_{5,6}\,(\pm x_5, 0, \pm y_5, 0, \pm z_5, 0)$ $x_5 = \chi\left(1 - \beta_3 + \beta_2\beta_3 - \alpha + \alpha\beta_2 - \alpha^2\right)$ $y_5 = \chi\left(1 + \beta_1 - \beta_1\beta_3 + \alpha + \alpha\beta_3 + \alpha^2\right)$ $z_5 = -1 - \alpha x_5 + \beta_2 y_5$	
$E_{7,8}\,(\pm x_7, 0, \pm y_7, 0, \pm z_7, 0)$ $x_7 = \chi\left(1 - \beta_3 + \beta_2\beta_3 - \alpha + \alpha\beta_2 - \alpha^2\right)$ $y_7 = \chi\left(1 + \beta_1 - \beta_1\beta_3 + \alpha + \alpha\beta_3 + \alpha^2\right)$ $z_7 = -1 - \alpha x_7 + \beta_2 y_7$	
$E_{9,10}\,(\pm x_9, 0, \pm y_9, 0, \pm z_9, 0)$ $x_9 = \chi\left(\alpha^2 + \beta_3\right)$ $y_9 = \chi\,(\beta_1\beta_3 - \alpha)$ $z_9 = 1 - \alpha x_9 + \beta_2 y_9$	$\mathrm{k}_5 = 3\delta$ $k_4 = 3\delta^2$ $k_3 = \delta^3$ $k_2 = \alpha\beta_1 - 2\alpha\beta_2 - 2\alpha\beta_3 - 3,$ $k_1 = \delta\,(-2\alpha\beta_3 + \alpha\beta_1 - 2\alpha\beta_2 - 3),$ $k_0 = 2\alpha\beta_1 + 2\alpha\beta_2 + 2\alpha\beta_3 + 2\alpha^3 - 2\beta_1\beta_2\beta_3 + 2$ ($k_5k_0 < 0$ unstable)
$E_{11,12}\,(\pm x_{11}, 0, \pm y_{11}, 0, \pm z_{11}, 0)$ $x_{11} = \chi\left(-\alpha^2 + \beta_2\beta_3\right)$ $y_{11} = \chi\,(1 + \alpha\beta_3)$ $z_{11} = -\alpha x_{11} + \beta_2 y_{11}$	$k_5 = 3\delta$ $k_4 = 3\delta^2$ $k_3 = \delta^3$ $k_2 = -2\alpha\beta_1 - 2\alpha\beta_2 + \alpha\beta_3 - 3$ $k_1 = \delta\,(\alpha\beta_3 - 2\alpha\beta_1 - 2\alpha\beta_2 - 3)$ $k_0 = 2\alpha\beta_1 + 2\alpha\beta_2 + 2\alpha\beta_3 + 2\alpha^3 - 2\beta_1\beta_2\beta_3 + 2$ ($k_5k_0 < 0$ unstable)
$E_{13,14}\,(\pm x_{13}, 0, \pm y_{13}, 0, \pm z_{13}, 0)$ $x_{13} = \chi\,(1 + \alpha\beta_2)$ $y_{13} = \chi\left(\alpha^2 + \beta_1\right)$ $z_{13} = -\alpha x_{13} + \beta_2 y_{13}$	$k_5 = 3\delta$ $k_4 = 3\delta^2$ $k_3 = \delta^3$ $k_2 = -2\alpha\beta_1 + \alpha\beta_2 - 2\alpha\beta_3 - 3$ $k_1 = \delta\,(-2\alpha\beta_3 - 2\alpha\beta_1 + \alpha\beta_2 - 3)$ $k_0 = 2\alpha\beta_1 + 2\alpha\beta_2 + 2\alpha\beta_3 + 2\alpha^3 - 2\beta_1\beta_2\beta_3 + 2$ ($k_5k_0 < 0$ unstable)

reported the chaotic attractors captured experimentally for three different sets of parameters (Figure 11a, c, and e) and related results (Figure 11b, d, and f) obtained from a direct numerical integration of the network Equations

Equilibrium point	Stability type
$E_{15,16}\,(\pm x_{15}, 0, \pm y_{15}, 0, \pm z_{15}, 0)$	
$x_{15} = \chi\left(\beta_3 + \beta_2\beta_3 - \alpha + \alpha^2\right)$	
$y_{15} = \chi\left(1 - \alpha + \beta_1\beta_3 + \alpha\beta_3\right)$	
$z_{15} = 1 - \alpha x_{15} + \beta_2 y_{15}$	$k_5 = 3\delta$
	$k_4 = 3\delta^2 + 3$
$k_3 = \delta^3 + 6\delta$,	$k_2 = 3\delta^2 + \alpha\left(-2\beta_1 + 4\beta_2 - 2\beta_3\right)$,
	$k_1 = \delta\left(4\alpha\beta_2 - 2\alpha\beta_1 - 2\alpha\beta_3\right)$,
	$k_0 = 4\beta_1\beta_2\beta_3 - 4\alpha\beta_2 - 4\alpha\beta_3 - 4\alpha^3 - 4\alpha\beta_1 - 4$
	($k_5k_0 < 0$ unstable)
$E_{17,18}\,(\pm x_{17}, 0, \pm y_{17}, 0, \pm z_{17}, 0)$	
$x_{17} = \chi\left(-\beta_3 + \beta_2\beta_3 - \alpha - \alpha^2\right)$	
$y_{17} = \chi\left(1 + \alpha - \beta_1\beta_3 + \alpha\beta_3\right)$	
$z_{17} = -1 - \alpha x_{17} + \beta_2 y_{17}$	
$E_{19,20}\,(\pm x_{19}, 0, \pm y_{19}, 0, \pm z_{19}, 0)$	
$x_{19} = \chi\left(1 + \beta_3 + \alpha\beta_2 + \alpha^2\right)$	
$y_{19} = \chi\left(\beta_1 - \alpha + \beta_1\beta_3 + \alpha^2\right)$	
$z_{19} = 1 - \alpha x_{19} + \beta_2 y_{19}$	
	$k_6 = 1$,
	$k_5 = 3\delta$,
	$k_4 = 3\delta^2 + 3$,
	$k_3 = \delta^3 + 6\delta$,
	$k_2 = 3\delta^2 + \alpha\left(-2\beta_1 - 2\beta_2 + 4\beta_3\right)$,
	$k_1 = \delta\left(4\alpha\beta_3 - 2\alpha\beta_1 - 2\alpha\beta_2\right)$,
	$k_0 = -4\alpha\beta_1 - 4\alpha\beta_2 - 4\alpha\beta_3 - 4\alpha^3 + 4\beta_1\beta_2\beta_3 - 4$
	($k_5k_0 < 0$ unstable)
$E_{21,22}\,(\pm x_{21}, 0, \pm y_{21}, 0, \pm z_{21}, 0)$	
$x_{21} = \chi\left(1 - \beta_3 + \alpha\beta_2 - \alpha^2\right)$	
$y_{19} = \chi\left(\beta_1 + \alpha - \beta_1\beta_3 + \alpha^2\right)$	
$z_{21} = -1 - \alpha x_{21} + \beta_2 y_{21}$	
$E_{23,24}\,(\pm x_{21}, 0, \pm y_{21}, 0, \pm z_{21}, 0)$	
$x_{23} = \chi\left(1 - \alpha + \alpha\beta_2 + \beta_2\beta_3\right)$	
$y_{23} = \chi\left(1 + \beta_1 + \alpha\beta_3 + \alpha^2\right)$	
$z_{23} = -\alpha x_{23} + \beta_2 y_{23}$	$k_5 = 3\delta$
	$k_4 = 3\delta^2 + 3$
	$k_3 = \delta^3 + 6\delta$
	$k_2 = 3\delta^2 + \alpha\left(4\beta_1 - 2\beta_2 - 2\beta_3\right)$
	$k_1 = \delta\left(4\alpha\beta_1 - 2\alpha\beta_2 - 2\alpha\beta_3\right)$
	$k_0 = -4\alpha\beta_1 - 4\alpha\beta_2 - 4\alpha\beta_3 - 4\alpha^3 + 4\beta_1\beta_2\beta_3 - 4$
	($k_5k_0 < 0 \Rightarrow$unstable)
$E_{25,26}\,(\pm x_{25}, 0, \pm y_{25}, 0, \pm z_{25}, 0)$	
$x_{25} = \chi\left(1 + \alpha + \alpha\beta_2 - \beta_2\beta_3\right)$	
$y_{25} = \chi\left(-1 + \beta_1 - \alpha\beta_3 + \alpha^2\right)$	
$z_{25} = -\alpha x_{25} + \beta_2 y_{25}$	

Note: We introduce $\chi = ($ and assume . The group of equilibrium points share the same stability property and undergo Hopf-type bifurcation with the variation of a chosen control parameter.

(4)–(9) with the same set of parameters: Figure 11a and b for $\alpha = 0.6$, $\beta_1 = 0.6$, $\beta_2 = \beta_3 = 0$, and $\delta = 0.6$; Figure 11c and d for $\alpha = 0.6$, $\beta_1 = \beta_2 = 0.6$, $\beta_3 = 0$, and ; and Figure 11e and f for $\alpha = 0.6$, $\beta_1 = \beta_2 = \beta_3 = 0.6$, $\delta = 0.6$. The very good agreement observed between the theoretical phase portraits and those recorded experimentally serves to validate the theoretical study reported in the present work.

5. Conclusion

This work focused on the collective dynamics of a ring network comprising three mutually interacting twin-well DOs. Both analytical and numerical methods were employed to shed light on the collective behavior of the network with respect to its parameters (i.e., coupling factors, dissipation parameter). We showed that the route to multi-scroll chaos starts with a sequence of Hopf bifurcations associated with 8 of the 27 equilibrium points, followed by a sequence of period-doublings, extinction crises, and fusion, ultimately giving rise to the multi-scroll attractor when one of the parameters (e.g., a coupling strength) changes monotonically. We reported various zones of multi-stability where several attractors of different topologies coexist in varied numbers, depending on the value of the control parameter. This scenario was elucidated by applying bifurcation diagrams, phase portraits, and basins of attraction. Moreover, reducing the number of interactions in the underlying network was accompanied by a profound modification of the positions of the equilibrium points, the mechanism resulting in chaos, and the structure of the final multi-scroll attractor. An experimental study was conducted using an Arduino microcontroller board.

The multi-scroll chaotic signal reported in this work has the potential to be applied in engineering fields, such as image encryption, chaotic mixing, and robot control. Moreover, the results obtained in this article provide the basic information necessary for understanding a more

complex network of coupled DOs. The impact of time delay coupling and the fractional order on the dynamics of the network studied in this work can be explored in future studies.

Acknowledgments

None.

Funding

None.

Conflict of interest

Kengne Jacques is an Editorial Board Member of this journal, but was not in any way involved in the editorial and peer-review process conducted for this paper, directly or indirectly. The other authors declare no competing interests.

Author contributions

Conceptualization: Chedjou Jean Chamberlain
Formal analysis: Mahirakhon Rakhmatullaeva, Khabibulo Nosirov, Kengne Jacques
Investigation: Mahirakhon Rakhmatullaeva, Khabibulo Nosirov, Kengne Jacques
Methodology: Chedjou Jean Chamberlain
Writing–original draft: All authors
Writing–review & editing: All authors

Availability of data

All data analyzed have been presented in the paper.

AI Tools Statement

All authors confirm that no AI tools were used in the preparation of this manuscript.

References

1. Mahmoudvand S, Ghazavi MR, Farrokhabadi A. Nonlinear dynamic modeling and chaos analysis of aircraft landing gear under two-and three-point landings. *Nonlinear Sci Control Eng.* 2025;1(1):025280001. http://dx.doi.org/10.36922/NSCE025280001
2. Boccaletti S, Latora V, Moreno Y, et al. Complex networks: structure and dynamics. *Phys Rep.* 2006;424(4–5):175–308. http://dx.doi.org/10.1016/j.physrep.2005.10.009
3. Pippal S, Kapoor S, Ranga A. Bifurcation and stability analysis with numerical simulations of a social model for marriage and divorce under fear effect. *Nonlinear Sci Control Eng.* 2025;1(1):025290005. http://dx.doi.org/10.36922/NSCE025290005
4. Ugur E, Toktaş A, Toktaş F, et al. Hybridization of benchmark functions for a high-performance 1D chaotic map and image encryption application. *Nonlinear Sci Control Eng.* 2025;1(1):025340010. http://dx.doi.org/10.36922/NSCE025340010
5. Terman D, Wang D. Global competition and local cooperation in a network of neural oscillators. *Physica D.* 1995;81(1-2):148-176. http://dx.doi.org/10.1016/0167-2789(94)00205-5
6. Pietra B, Daffertshofer A. Network dynamics of coupled oscillators and phase reduction techniques. *Phys Rep.* 2019;819:1-105. http://dx.doi.org/10.1016/j.physrep.2019.06.001
7. Duffing G. *Erzwungene Schwingungen bei veränderlicher Eigenfrequenz und ihre technische Bedeutung.* Vieweg; 1918.
8. Tchakui MV, Woafo P. Dynamics of three unidirectionally coupled autonomous Duffing oscillators and application to inchworm piezoelectric motors: effects of the coupling coefficient and delay. *Chaos.* 2016;26(11):113108. http://dx.doi.org/10.1063/1.4967388
9. Leo Kingston S, Kapitaniak T, Dana SK. Transition to hyperchaos: Sudden expansion of attractor and intermittent large-amplitude events in dynamical systems. *Chaos.* 2022;32(8):083101. http://dx.doi.org/10.1063/5.0108401
10. Sabarathinam S, Thamilmaran K. Transient chaos in a globally coupled system of nearly conservative Hamiltonian Duffing oscillators. *Chaos Solitons Fractals.* 2015;73:129-140. http://dx.doi.org/10.1016/j.chaos.2015.01.004
11. Jaimes-Reátegui R, Castillo-Cruz JM, Garcıa-López JH, et al. Self-organization in network motifs of three bistable Duffing oscillators. *Cybern Phys.* 2020;9(1):31-40. http://dx.doi.org/10.35470/2226-4116-2020-9-1-31-40
12. Musielak D, Musielak Z, Benner J. Chaos and routes to chaos in coupled Duffing oscillators with multiple degrees of freedom. *Chaos Solitons Fractals.* 2005;24(4):907-922. http://dx.doi.org/10.1016/j.chaos.2004.09.119
13. Clerc MG, Coulibaly S, Ferré MA, et al. Chimera states in a Duffing oscillators chain coupled to nearest neighbors. *Chaos.* 2018;28(8):083115. http://dx.doi.org/10.1063/1.5025038
14. Jothimurugan R, Thamilmaran K, Rajasekar S, et al. Multiple resonance and anti-resonance in coupled Duffing oscillators. *Nonlinear Dyn.* 2016;83:1803-1814. http://dx.doi.org/10.1007/s11071-015-2447-9
15. Jaros P, Kapitaniak T, Perlikowski P. Multistability in nonlinearly coupled ring of Duffing systems. *Eur Phys J Spec Top.* 2016;225:2623–2634. http://dx.doi.org/10.1140/epjst/e2016-60015-7
16. Borkowski L, Perlikowski P, Kapitaniak T, Stefanski A. Experimental observation of three-frequency quasiperiodic solution in a ring of unidirectionally coupled oscillators. *Phys Rev E Stat Nonlin Soft Matter Phys.* 2015;91:062906. http://dx.doi.org/10.1103/PhysRevE.91.062906
17. Barba-Franco JJ, Gallegos A, Jaimes-Reátegui R, et al. Dynamics of a ring of three unidirectionally coupled Duffing oscillators with time-dependent damping. *Europhys Lett.* 2021;134(3):30005. http://dx.doi.org/10.1209/0295-5075/134/30005
18. Balamurali R, Kengne LK, Rajagopal K, et al. Coupled non-oscillatory Duffing oscillators: multistability, multiscroll chaos generation and circuit realization. *Physica A.* 2022;607:128174. http://dx.doi.org/10.1016/j.physa.2022.128174
19. Pastor I, Pérez-García VM, Encinas F, et al. Ordered and chaotic behavior of two coupled van der Pol oscillators. *Phys Rev E.* 1993;48(1):171-176. http://dx.doi.org/10.1103/PhysRevE.48.171
20. Kengne J, Chedjou JC, Kom M, et al. Regular oscillations, chaos, and multistability in a system of two coupled van der Pol oscillators: numerical and experimental studies. *Nonlinear Dyn.* 2014;76:1119-1132. http://dx.doi.org/10.1007/s11071-013-1195-y
21. Singh AK, Yadava R. Transient motion and chaotic dynamics in a pair of van der Pol oscillators. *Eur Phys J Plus.* 2019;134(9):421. http://dx.doi.org/10.1140/epjp/i2019-12804-x
22. Strogatz SH. *Nonlinear Dynamics and Chaos: With Applications to Physics, Biology, Chemistry, and Engineering.* CRC Press; 2018. http://dx.doi.org/10.1201/9780429398490
23. Guckenheimer J, Holmes P. *Nonlinear Oscillations, Dynamical Systems, and Bifurcations of Vector Fields.* Vol. 42. Springer Science & Business Media; 2013. http://dx.doi.org/10.1007/978-1-4612-1140-2